Free-electron laser spectrum evaluation and automatic optimization

Niky Bruchon [a,*], Gianfranco Fenu [a], Giulio Gaio [b,*], Marco Lonza [b], Felice Andrea Pellegrino [a], Lorenzo Saule [a]

[a] Department of Engineering and Architecture, Università degli Studi di Trieste, 34127 Trieste, Italy
[b] Elettra Sincrotrone Trieste, 34149 Basovizza, Trieste, Italy

ARTICLE INFO

Keywords:
Free-electron laser
Optimization
Ascent-gradient
Stochastic-extremum-seeking
Control-system

ABSTRACT

The radiation generated by a seeded free-electron laser (FEL) is characterized by a high temporal coherence, which is close to the Fourier limit in the ideal case. The setup and optimization of a FEL is a non-trivial and challenging operation. This is due to the plethora of highly sensitive machine parameters and to the complex correlations between them. The fine tuning of the FEL process is normally supervised by physicists and is carried out by scanning various parameters with the aim of optimizing the spectrum of the emitted pulses in terms of intensity and line-width. In this article we introduce a novel quantitative method for the evaluation of the FEL spectrum via a quality index. Moreover, we investigate the possibility of optimization of the FEL parameters using this index as the objective function of an automatic procedure. We also present the results of the preliminary tests performed in the FERMI FEL focused on the effectiveness and ability of the automatic procedure to assist in the task of machine tuning and optimization.

1. Introduction

FERMI is a seeded free-electron laser (FEL) based on the high-gain harmonic generation scheme [1,2], producing intense and fully coherent photon pulses in the range 4–100 nm [3,4]. Defining the optimal FEL working point, which generates a photon beam with good intensity and spectral purity, is a very demanding task for the physicists tuning the machine prior the experiments. Moreover, during experiments the performance can vary due to machine changes required by the scientists or due to slow drifts of some critical parameters. A number of shot-by-shot feedback loops running at the machine repetition rate [5] have been implemented in the FERMI control system [6] to stabilize energy, trajectory and bunch length of the electron beam as well as the trajectory of the laser beam used for the seeding. However, some machine parameters are not directly controllable and the FEL performance has to be recovered with a new optimization.

In order to support the optimization process we are investigating the feasibility of a generic automatic tuning procedure based on the evaluation of the overall quality of the output FEL radiation. An automatic optimization algorithm would prove particularly useful in non-standard setups required by more complicated configurations such as the fresh bunch injection technique of FEL-2 [4] or in experiments involving emission of multiple pulses [7], multiple harmonics, or coherent control [8].

The problem of optimizing the performance is quite common in FEL accelerator driven machines. It is rather difficult to have a complete theoretical model of the FEL process including all the possible variables and the extreme sensitivity of its critical parameters. As a consequence, a general interest in optimization algorithms has grown in the FEL community in the recent years. A flexible optimization tool called OCELOT, developed at DESY and currently used at FLASH, combines the ability to deal with model-based and model-free systems [9,10]. Moreover, Bayesian optimization methods have been successfully tested at LCLS [11]. In both accelerators the optimization tools are mainly used to tune either quadrupoles or the electron beam trajectory. The objective function of the optimization procedure is usually the photon beam intensity with a penalization factor based on beam losses along the undulators chain [12].

At FERMI, automatic optimization methods have already been implemented in the past based on statistical analysis of shot-to-shot data [13]. However, they can only be applied to specific machine parameters such as the beams trajectory in order to maximize the photon beam intensity.

In the present work we define a quality index based on the observation of the FEL spectrum, with the idea of using it as objective function of a generic automatic optimization process. The main on-line non-destructive diagnostic available is a high resolution photon energy

* Corresponding authors.
E-mail addresses: br.niky@gmail.com (N. Bruchon), giulio.gaio@elettra.eu (G. Gaio).

Accepted 24 July 2017

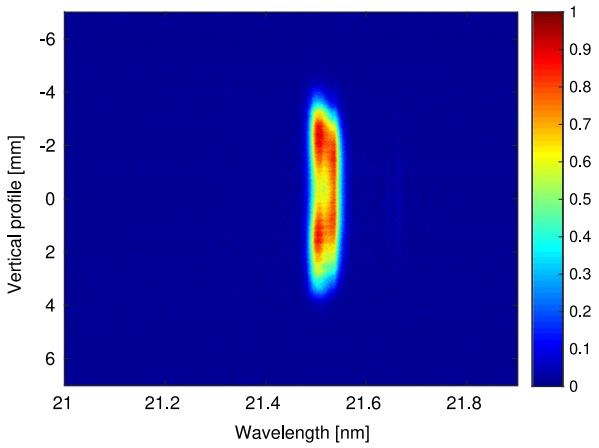

Fig. 1. Example of spectrum image. The values reported in the colorbar correspond to the normalized intensity of the photons. The same colorbar is also used in the other images of the paper.

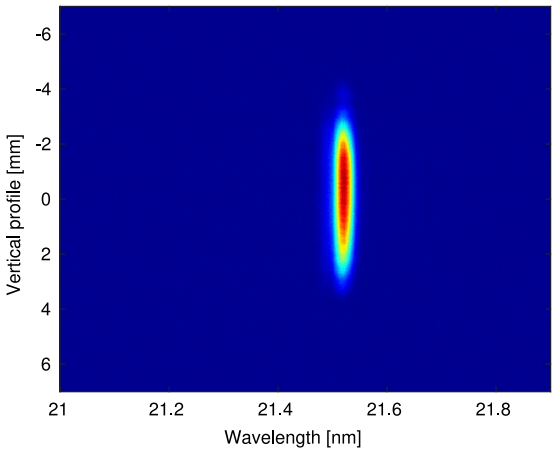

Fig. 2. Example of a good quality spectrum with a single, horizontally narrow and intense spot.

spectrometer, capable of measuring shot by shot the spectral content of each emitted photon pulse [14]. The spectrometer covers all the FERMI radiation range by using three selectable diffraction gratings. The zero-order beam (97% of the photons) is sent to the experimental stations while the first order is focused onto an Yttrium Aluminum Garnet (YAG) screen and the fluorescence intensity is detected by a Charge Coupled Device (CCD) by Hamamatsu. As a result an image representing the actual spectrum is produced (Fig. 1).

In presence of an ideal spectrum, the horizontal projection of the image resembles a spectral line with Gaussian distribution and bandwidth as narrow as $\Delta\lambda/\lambda = 1 \times 10^{-3}$ (fwhm) or less. The vertical projection represents instead the transverse vertical photon beam distribution. The acquired spectrometer image is represented by a 1000×1000 matrix where the columns correspond to different values of wavelength and the rows correspond to a vertical position on the CCD.

2. FEL quality factor

The manual tuning of the machine during the FEL preparation is routinely performed by looking at the spectrum image and adjusting some parameters until the spectrum is satisfactory. The parameters involved in manual spectrum optimization can be divided in two categories: the ones which are tuned after a wavelength change and are definitively not subject to drifts and the ones which have to be periodically tuned to maintain optimal the FEL output.

In the first category there are (with the maximum tolerable change):

- dispersive section, R56 (2% $\Delta I/I$);
- laser heater power (5% $\Delta E/E$);
- ondulator tapering (0.1% $\Delta E/E$);
- LINAC energy (0.1% $\Delta E/E$).

In the second category there is:

- delay between electrons and seed laser (100 fs).

We propose a quality index, referred as FEL quality factor (FelQFactor), able to evaluate the beam quality by analyzing the spectrum image [15]. The index is designed to produce high values when the spectrum shape is close to a single, horizontally narrow and intense spot (Fig. 2). Conversely the index is negatively affected by a spectrum composed by multiple peak areas, a wide central spectral line and low intensity. A fundamental requirement for this index is to evaluate the FEL spectral quality like a machine expert would; in other words, given two spectra A and B, such that A is considered better than B by an expert, FelQFactor(A) should be higher than FelQFactor(B).

In this section, we first define a parametric family of candidate functions. Then, based on a set of image spectra ordered according to the ranking given by experts, we find out a function that produces the most similar ranking.

The first step for computing the FelQFactor consists in detecting each peak area of the image using a novel procedure inspired by the Maximally Stable Extremal Regions (MSER) algorithm [16].

The algorithm creates a binary image which has the same size of the original spectrum image and whose pixels are set respectively to 0 or 1 when the corresponding pixel value is below or above a given threshold. In order to filter out the noise from the image, a background level (the level below which the pixels are not taken into account) is fixed to $\alpha \cdot max_{pixel\ level}$ $(0.1 < \alpha < 0.3)$. Then a number of N evenly spaced threshold levels ($N \geq 20$) between the background and the maximum value are calculated. In the first step of the algorithm the threshold is set at the maximum level; as a consequence the binary image is empty. When the threshold level decreases to the next lower value, the number of pixels above threshold increases and the first peak areas (groups of pixels touching each other with no gaps in between) start to appear and gradually expands in size at each subsequent step. When two or more areas which contain a number of pixels above a given threshold ($\geq$1000 pixels) start merging with each other (which happens when the pixels belonging to different peak areas in the previous step become part of the same peak area at the current step) the pixels of the two merging areas are no more taken into account in the thresholding process and are separately stored. An example is reported in Fig. 3: by lowering the threshold, the two areas visible in Fig. 3(a) get merged in a single area as shown in Fig. 3(b).

The result of this process is a set of images each corresponding to a single peak area. In Fig.4 the picture on the left is the original spectrum image, while on the right side the image containing the peak areas memorized in the data structure is shown.

The subsequent processing phase is the extraction of two categories of features from the data structure:

- features of the image as a whole: total number of peak areas, number of peak areas not overlapped in the horizontal projection, number of peak areas not overlapped in the vertical projection;
- specific features of each peak area: total area, coordinates of the centroid, horizontal and vertical dimensions, intensity (sum of all the pixel values).

The FelQFactor proposed in this work is the product of two functions named I and F. The function I takes into account the intensity and the shape of the peak featuring the highest total intensity. Two variants of I are considered:

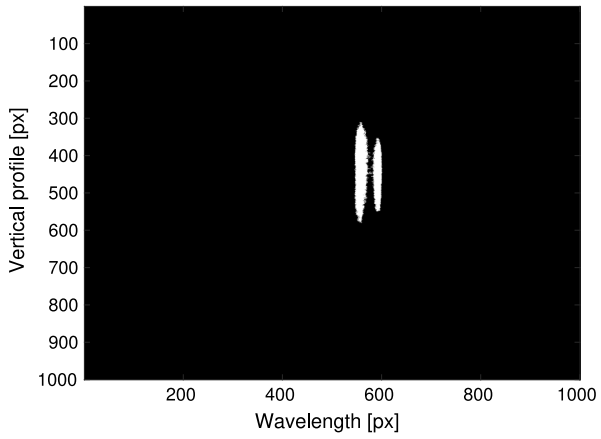

(a) Peak areas before merging.

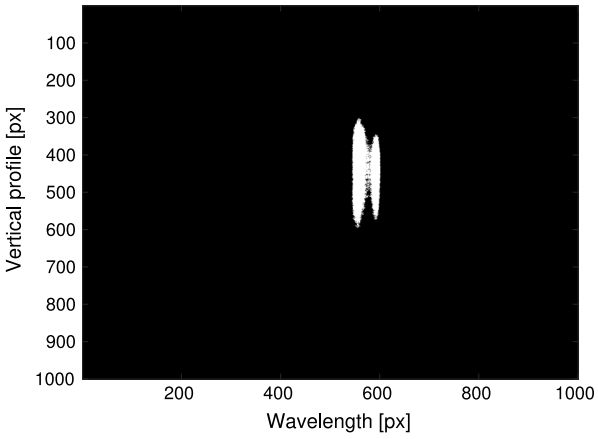

(b) Peak areas after merging.

Fig. 3. Peak areas detection in spectrum thresholding.

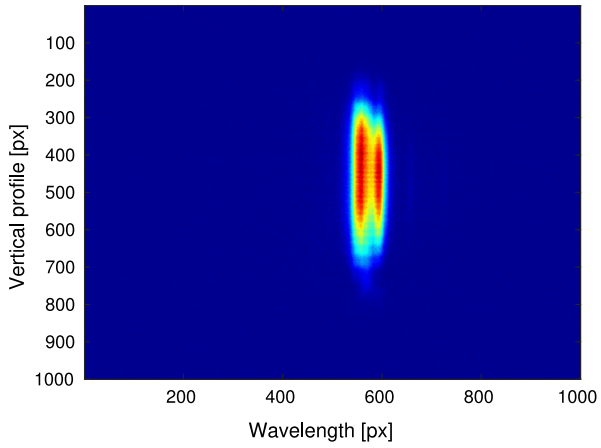

(a) Spectrum image.

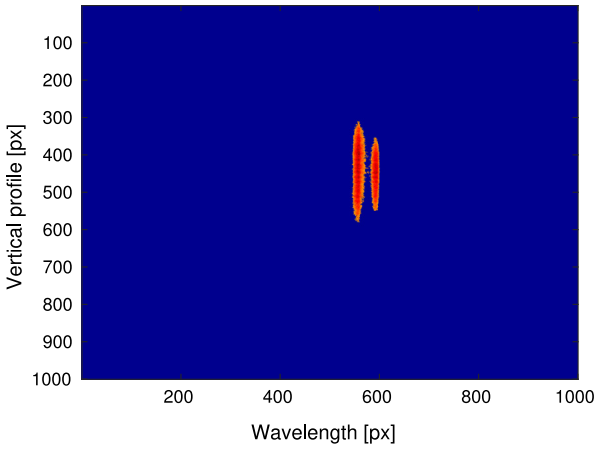

(b) Image containing the peak areas.

Fig. 4. Example of extraction of peak areas from a spectrum image.

- $I_1 = \frac{(J_{Tot})^a}{\sigma_H^b \cdot \sigma_V^c}$
- $I_2 = \frac{(J_{Tot})^a}{\left(\frac{\sigma_H}{\sigma_{0H}}\right)^b + \left(\frac{\sigma_V}{\sigma_{0V}}\right)^c}$

J_{Tot}, σ_H and σ_V are respectively the total intensity (the sum over the whole area), the horizontal and the vertical dimensions of the most intense peak area. σ_{0H} and σ_{0V} correspond to the dimensions of a reference spectrum obtained by averaging a set of "good" spectra selected by machine experts. Exponents a, b and c are integer values belonging to the set $\{1, 2, 3\}$.

The function F takes into account the number and the arrangement of the energy peak areas. Three variants are considered:

- $F_1 = \left(\frac{1}{N_T}\right)^k$
- $F_2 = \left(\frac{1}{N_H + N_V}\right)^k$
- $F_3 = \left(\frac{J_{Max}}{\sum_{i=0}^{n-1} J_i}\right)^k$

N_T is the total number of image peak areas, N_H and N_V are respectively the number of peak areas visible on the horizontal and vertical projection. J_i are the intensity of the n peaks found in the image, while J_{Max} is the intensity of the peak area with the highest total intensity. The exponent k is an integer value belonging to the set $\{1, 2, 3\}$.

The FelQFactor index is given by the base-10 logarithm of the product between an I function and an F function. The following notation is used to identify the family of functions:

$$I_m F_n(a, b, c, k) \tag{1}$$

where m, n, a, b, c, k are the function parameters.

In order to find the FelQFactor function parameters that evaluate the FEL spectrum similarly to how the physicists would do, a dataset of 800 real spectrum images has been acquired in different machine conditions. A subset of 30 images which well represents the transition from the worst to the best spectrum has been ranked by the physicists in terms of quality and set as a reference.

The same subset of spectra has been sorted by all the 486 possible combinations of the FelQFactor function. Spearman's footrule [17] has been used to measure the mismatch between the reference list and the ranking produced by the FelQFactor functions.

$$F(\delta) = \sum_{i=1}^{n} |i - \delta(i)| \tag{2}$$

where i is the image rank in the reference list, while $\delta(i)$ is its rank produced by the FelQFactor function.

The 16 functions featuring the best score have been chosen for a further evaluation process. Each of them has been then used to sort the full set of 800 images based on the FelQFactor value and the result of

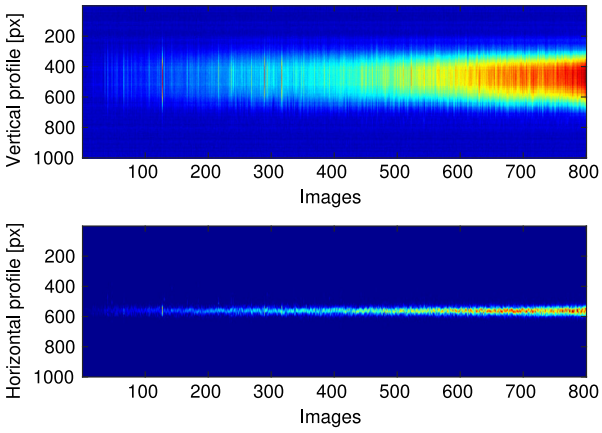

(a) Spectral profiles: each of the 800 sorted images is projected, summing all the row (column) values, into a vector; all these vectors are then placed side by side into this vertical (horizontal) spectral profile.

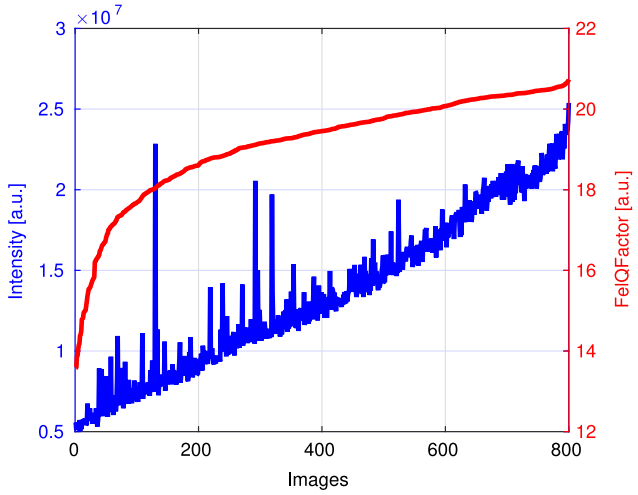

(b) FelQfactor and intensity of the spectra used to create the profiles shown in Fig. 5(a). The intensity peaks are due to the high sensitivity in peak areas detection of the MSER algorithm.

Fig. 5. Results of the 800 images sorting using function $I_2F_2(3,1,2,1)$.

the sorting has been visually evaluated by the experts who have finally selected the best function, which is:

$$I_2F_2(3,1,2,1) = \log_{10}\left(\frac{(I_{Tot})^3}{\left(\frac{\sigma_H}{\sigma_0 H}\right)^1 + \left(\frac{\sigma_V}{\sigma_0 V}\right)^2} \cdot \left(\frac{1}{N_H + N_V}\right)^1\right). \quad (3)$$

Fig. 5 gives a visual representation of the efficacy of the above method to sort all the 800 FEL spectra images. The sort in Fig. 5(a), which is considered by the physicists the best among the ones produced by the 16 functions, show that spectra with good intensity and shape are placed on the right side of the sequence. The values of intensity and FelQfactor for each spectrum are reported in Fig. 5(b) respectively in blue and red.

When testing FelQFactor we noticed that it is affected by the underlying noise of the spectral images. In order to strengthen the algorithm, an additional median filter applied to groups of five consecutive images has been included in the algorithm used during the experiments described below.

The image processing program to calculate the FelQFactor has been developed in C/C++, while Matlab scripts have been used for testing the algorithm and analyzing the results.

At present, the computational burden for calculating the FelQFactor from 1000×1000 pixel spectrum images limits the repetition rate to 2 Hz. To overcome this limitation a less computationally intensive version of the algorithm is under study. The goal is to be eventually able to process shot-by-shot data in real-time at the FERMI repetition rate of 50 Hz.

3. Optimization of FelQFactor

Given the objective function as in eq (3), the aim is tuning the machine parameters to maximize its value. As a first simple attempt to exploit the FelQFactor for tuning purposes, we assume that no *a priori* knowledge is available about the effect of the tunable parameters on the value achieved by eq (3). Usually, this is not the case because the machine experts are aware of the meaning and effect of the parameters and their interactions. However, in the experiments reported here, we intentionally do not use such information. As a consequence, we are facing an optimization problem in which the objective function can only be evaluated but whose dependency on the decision variables is not known. The approaches we have considered are the *ascent gradient* and the *stochastic extremum seeking* [18].

The software to implement the algorithms has been developed in-house using Matlab.

3.1. Ascent gradient

Ascent gradient is a first-order iterative optimization algorithm. In order to find a local maximum of a function $f(x)$, the input value is changed proportionally to the gradient of the function in the current point.

The ascent gradient algorithm starts from an arbitrary point x_0 and proceeds by iteratively updating its value according to the law $x_i = x_{i-1} + \alpha_{i-1} \cdot \nabla f(x_{i-1})$, where α determines the convergence speed to approach the final solution.

The ascent gradient method requires the full knowledge of the function to be optimized, but this is not always possible. If the function is not known in advance, but its value can be measured on the system for each input, a gradient approximation can be considered:

$$\nabla \approx \frac{f(x_i) - f(x_{i-1})}{x_i - x_{i-1}} \quad (4)$$

where two consecutive values of x and $f(x)$ are needed.

Due to the presence of noise in the real system, the algorithm we have implemented fixes α to 1 and moves the input variable with fixed steps to avoid instabilities. Starting from x_0 the system output $f(x_0)$ is acquired. At the first iteration the input is moved in an arbitrary direction, then the direction is given by the sign of the approximate gradient. The number of iterations, *iter_num*, is established in advance.

3.2. Extremum seeking

Perturbation driven extremum seeking is a well known technique for finding and maintaining the extremal value of an unknown function (see for instance the overview [19] and the dedicated book chapter [20] for a general overview of the method). Many different classes of extremum seeking schemes have been proposed in years, starting from the application of deterministic periodic perturbations (see [20] and the references therein) for continuous-time systems, extensions to the discrete time case [21] and the recent [22], to stochastic perturbations [23,24] and parameter uncertainties [25]. Recently an extremum seeking control strategy, based on the so called Control Lyapunov Functions (CLFs) theory, has been proposed [26,27] and successfully applied to optimize the performance and predict multiple parameter values in several particle accelerator applications [28–31] and the very recent [32].

In the proposed method, we implement a classic stochastic extremum seeking scheme, as in [23], for a static scalar plant, as depicted in Fig. 6. The output of the "non linear map" is, in facts, the current value of the FelQfactor, whereas the θ parameter is the plant parameter to be optimized. A detailed description of the extremum seeking approach is far beyond the scope of this paper. We only say that the stochastic

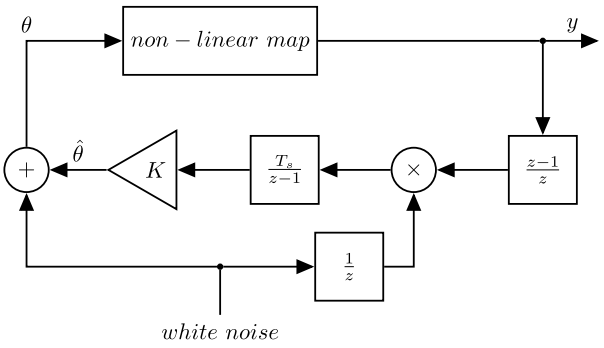

Fig. 6. Scheme of the applied extremum seeking technique (T_s is the sampling time; the block $\frac{T_s}{z-1}$ is an approximate discrete time integrator, K is a scalar gain, the block $\frac{1}{z}$ is a unity delay whereas the block $\frac{z-1}{z}$ is an approximate discrete time differentiator).

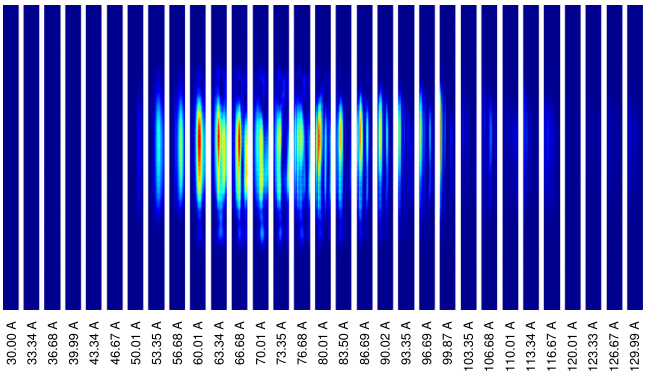

Fig. 7. Sequence of spectra for different dispersive section currents; the best spectrum is at about 60 A. The horizontal and vertical axis of each image are the wavelength and the vertical position.

extremum seeking is based on the injection of a perturbation signal (the white noise in Fig. 6). Such perturbation contributes by addition to the input for the static nonlinear map. A "washout" filter[1] is then applied to the measured output y, eliminating, as practical useful result, the eventually present DC component of the static map output. The resulting signal is then multiplied by the same perturbation signal, delayed of a single sampling time instant, generating an estimate of the scalar gradient of the nonlinear map at the input of the approximate discrete-time "integrator" block $\frac{T_s}{z-1}$ (where T_s is the sampling time). The "integrator" block updates the parameter estimate $\hat{\theta}$ in the direction of driving the gradient to 0. In particular, if $K > 0$ then the extremum seeking scheme drives $\hat{\theta}$ towards the nearest minimum of the nonlinear map, whereas for $K < 0$ the scheme converges to the nearest maximum of the map. The scheme in Fig. 6 has two design parameters: the integrator gain K influences the speed of convergence, whereas the white noise amplitude a provides a trade-off between asymptotic performance and algorithm region of attraction. In facts, the smaller the noise amplitude, the larger the possibility of getting stuck in a local minimum; on the contrary, the larger the noise amplitude, the larger the possibility of reaching the global minimum (for more details, the reader may refer to [21,23,24]).

4. Simulations

A series of simulations has been carried out using spectrum images acquired at FERMI by scanning the dispersive section. Fig. 7 is an example of consecutive spectrum images each corresponding to an actuator value. The actuator is changed in steps of 3.33 A; a narrow portion of each spectrum image around the main spectral line is extracted and all the images are placed side by side in the shown picture

The spectra dataset of the dispersive magnet current scan has been obtained by acquiring 50 images of the FEL spectrum for each magnet current. A simulator written in C/C++ loads the dataset and returns randomly one of the 50 spectrum images for each magnet current.

To evaluate the relationship between the dispersive magnet current and the FelQFactor, several scans have been simulated (Fig. 8).

Looking at the results two considerations can be made:

- The FelQFactor is quite noisy at the borders of the scan because of the drop of the FEL intensity which mixes up the blurring spectral lines with the CCD noise. In order to mitigate the noise, in the simulations and in the real case, the FelQFactor signal is filtered by means of a median filter.
- The absolute maximum of the FelQFactor corresponds roughly to a current value of 62 A but there is another region around 80 A which could trap the optimization algorithm because of its quasi-flat profile (local maximum).

[1] An high-pass filter, acting as approximate discrete-time "differentiator".

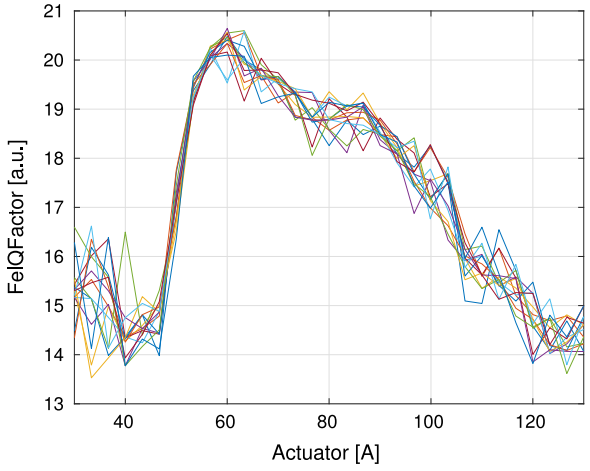

Fig. 8. FelQFactor vs. dispersive section current.

To evaluate the performance of the optimization process, two different starting points have been considered in these simulations:

- the first at 50 A, close to the rapid ascending slope of the curve towards the maximum to better evaluate the convergence speed of the algorithm;
- the second at 80 A in the middle of a flat region to verify the capability of the optimization process to avoid being trapped in a local maximum.

Both the considered algorithms have in common two parameters: the step size, which is fixed for the current implementation of the ascent gradient algorithm but changes within defined limits in the stochastic extremum seeking, and the so called integration gain, which affects directly the convergence speed of the algorithms and is equal to 1 in the ascent gradient method. A big step size can drive the optimization process rapidly to the optimum, with the drawback of increasing the noise once the optimum has been reached; a smaller step size, instead, produces less noise at steady state but a higher risk of being trapped in a local maximum. A higher integration gain speeds up the convergence but, when coupled with a large step size, could drive the algorithm to instability. On the other hand, a too small integration gain could prevent the algorithm from converging.

4.1. Ascent gradient

Before applying the optimizer on the real machine, a series of simulations with different step sizes has been done. In the Ascent Gradient method the sensitivity to step size variation has been analyzed.

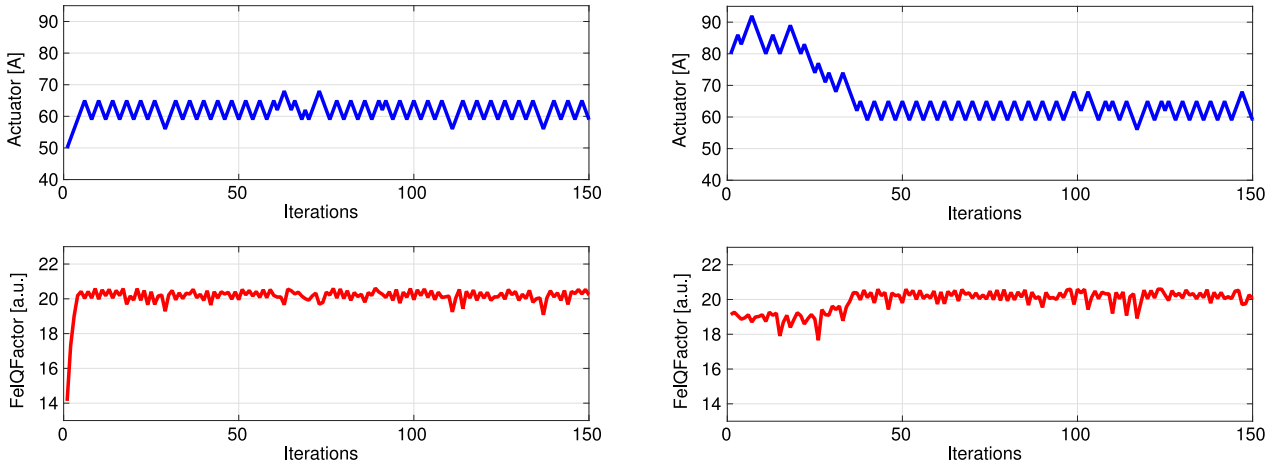

(a) Starting point 50 A.

(b) Starting point 80 A.

Fig. 9. Simulations of automatic optimization with the ascent gradient algorithm.

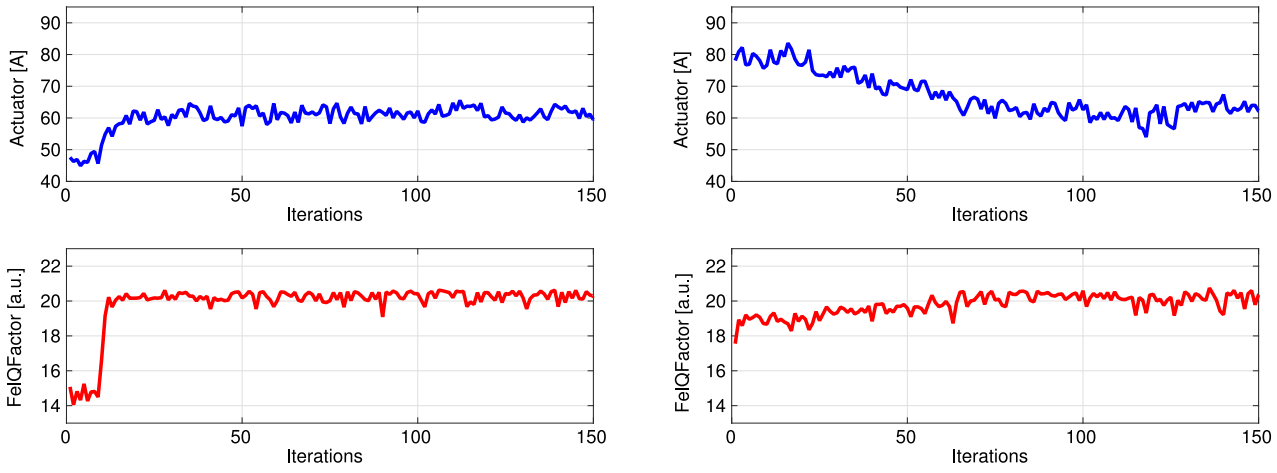

(a) Starting point 50 A.

(b) Starting point 80 A.

Fig. 10. Simulations of automatic optimization with the stochastic extremum seeking algorithm.

Table 1
FERMI parameters during experiments.

LINAC energy	1.1 GeV
electron bunch charge	700 pC
seed laser pulse duration	140 fs
seed laser pulse power	23 μJ
seed laser wavelength	261.5 nm
FEL wavelength	65.37 nm

We have considered the following values:

$$grad\_step \in \{\ 2.00,\ 2.50,\ 3.00,\ 3.50,\ 4.00\}\,.$$

Based on the convergence speed, the best choice for the step size is $grad\_step = 3.00$.

In Fig. 9 some simulation results obtained running the ascent gradient algorithm are shown.

4.2. Stochastic extremum seeking

The sensitivity analysis has been performed by means of a grid search on the two algorithm parameters: amplitude of the stochastic noise (a) and integrator gain (K). All the possible couples of parameter values in a given range are considered.

The values are:

$$a \in \{\ 2.00,\ 2.50,\ 3.00,\ 3.50,\ 4.00\ \},$$
$$K \in \{\ 0.50,\ 0.75,\ 1.00,\ 1.25,\ 1.50\ \}.$$

The parameter values that give the fastest convergence are $a = 3.00$ and $K = 1.00$.

The simulation results obtained running the stochastic extremum seeking algorithm are shown in Fig. 10.

The ascent gradient method is faster in reaching the best actuator value with both the starting points 50 A and 80 A, while the stochastic extremum seeking is roughly two times slower.

5. Application of the method in the FERMI FEL

The optimization algorithms have been tested on the FEL of FERMI. The Matlab code used for running the tests with the simulator has been adapted to be interfaced to the FERMI control system, thus allowing for direct driving of the actuators and reading of the FelQFactor calculated by the process in charge of the image spectrum evaluation.

The FERMI parameters during experiments are listed in Table 1.

5.1. Ascent gradient results

The ascent gradient algorithm iterations have been applied alternatively, with three steps for each, on the two actuators.

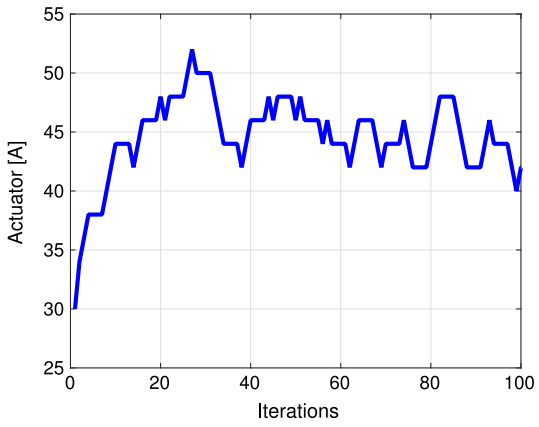

(a) Dispersive Section.

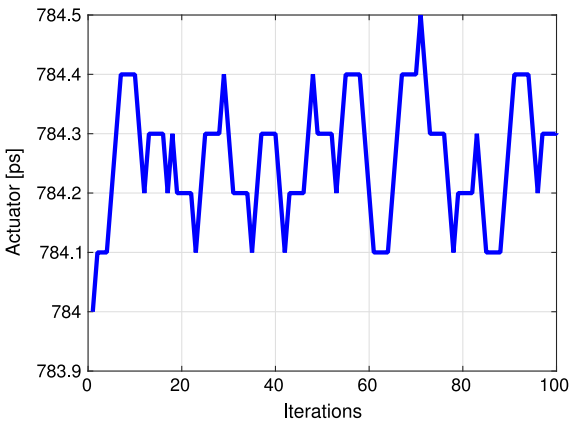

(b) Delay.

Fig. 11. Plots of the two actuators during the optimization with the ascent gradient.

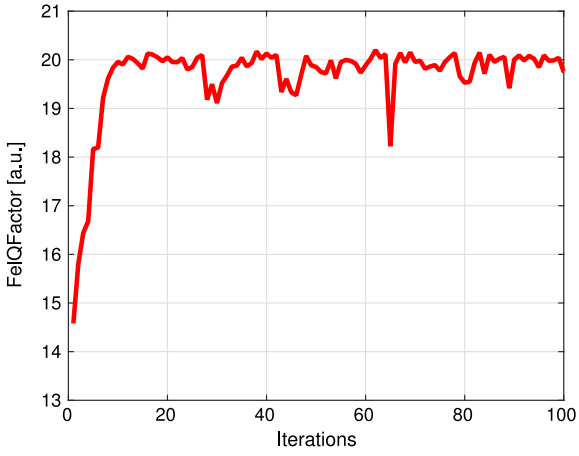

Fig. 12. FelQFactor during optimization with the ascent gradient.

The step sizes are:

$$grad\_step_{DispSect} = 2\ A; \qquad grad\_step_{Delay} = 0.1\ ps;$$

In Fig. 11, plots of the dispersive section current and the delay values during optimization are shown, while the FelQFactor improvement is depicted in Fig. 12.

Fig. 13 depicts the spectra before and after the optimization. In Fig. 14 the plots of the spectrum bandwidth and intensity during the test are shown.

5.2. *Stochastic extremum seeking results*

The values used for the algorithm parameters are:

$$a_{DispSect} = 1\ A; \quad a_{Delay} = 0.1\ ps;$$
$$K_{DispSect} = 2; \quad K_{Delay} = 0.1;$$

Similarly to the ascent gradient experiment, in Figs. 15 and 16 the results of the stochastic extremum seeking tests are reported, while the improvement of the spectrum is visible in Fig. 17. In Fig. 18 the plots of the spectrum bandwidth and intensity during the test are shown.

6. Conclusions

An automatic method to evaluate the quality of the FEL spectrum has been developed at FERMI; the quality index is called FelQFactor. It has been used as the objective function of two types of model-free optimization algorithms: ascent gradient and stochastic extremum seeking. Initially they have been tested in a simulated environment to

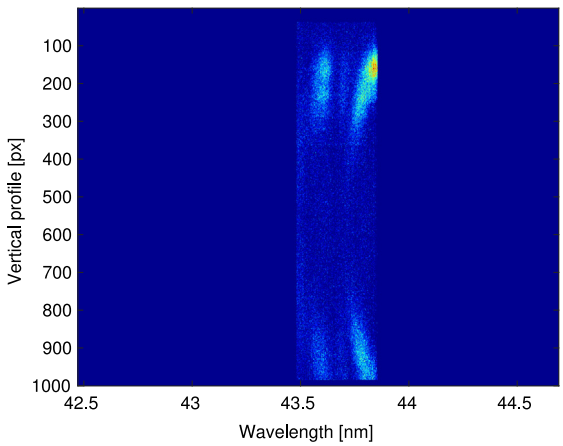

(a) Initial spectrum.

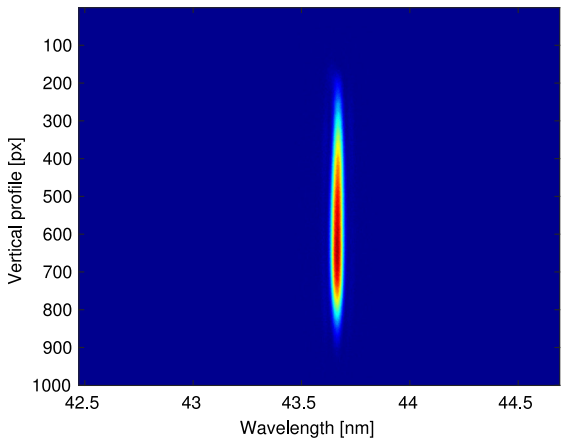

(b) Final spectrum.

Fig. 13. Spectrum before Fig 13(a) and after Fig 13(b) optimization with the ascent gradient method.

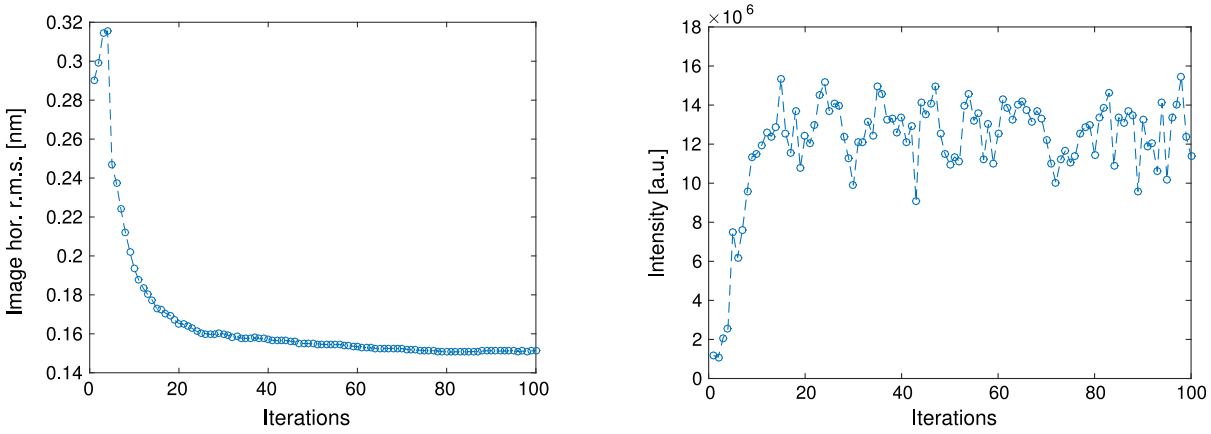

(a) Bandwidth.

(b) Intensity.

Fig. 14. Ascent gradient method: variation of spectrum bandwidth and intensity during the iterations.

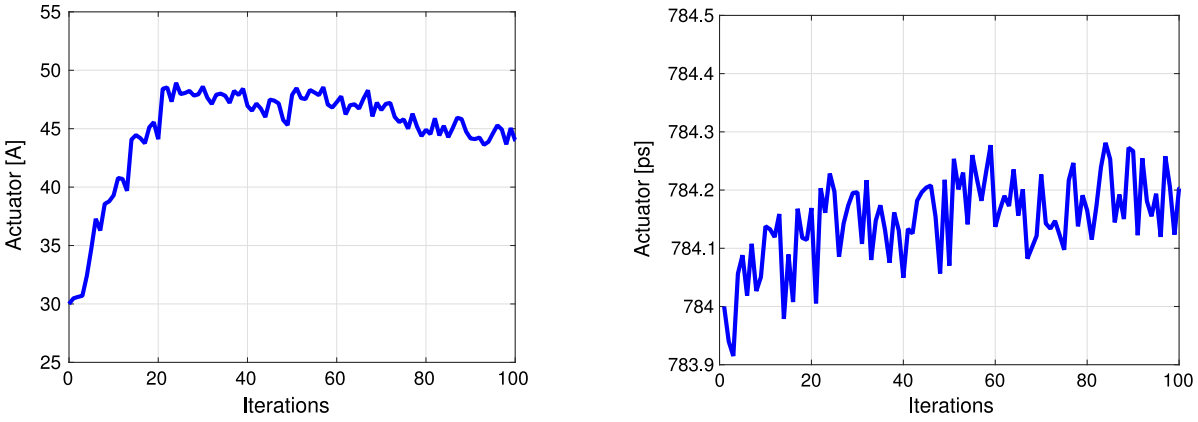

(a) Dispersive Section.

(b) Delay.

Fig. 15. Plots of the two actuators during the optimization with the stochastic extremum seeking.

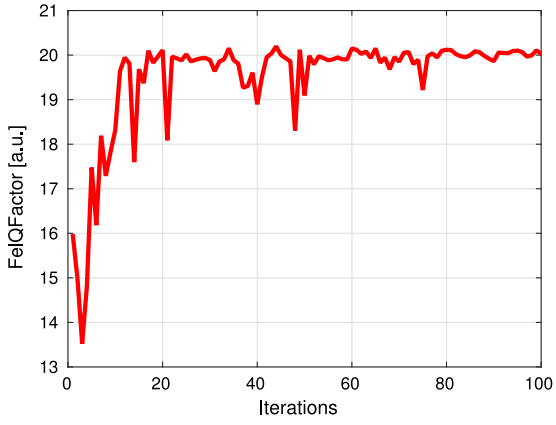

Fig. 16. FelQFactor during optimization with the stochastic extremum seeking.

verify their performance in the presence of noise and local maxima. A study on the sensitivity of the algorithm parameters has also been carried out to find the most effective values.

The ascent gradient and the stochastic extremum seeking optimization codes have then been tested on the real FEL machine.

At the end of both optimization processes, the usual variables considered by the scientists during FEL optimization (spectrum intensity, bandwidth and the overall spectrum shape) were improved. This is an encouraging indicator that the FelQFactor can be appropriate as an objective function in FEL tuning.

The goal of this work was to investigate the possibility of using automatic procedures to evaluate and optimize the FERMI FEL performance. The first results are promising and encourage us to continue with further efforts. The present FelQFactor algorithm is going to be refined based on the feedback from machine physicists and operators using it daily. For this purpose a graphical tool will be developed and made available in control room to be used as on-line FEL quality measurement. Further investigations are also foreseen on the optimization algorithms, especially on their capability to optimize concurrently multiple parameters, which could become the winning factor with respect to a manual optimization. However, the increase in the number of parameters is expected to bring a significant growth of the convergence time which could become incompatible with the machine preparation timing. For this reason a new implementation of the FelQFactor algorithm is under study, with the goal to be able to process every single photon pulse in real time at the full FEL repetition rate of 50 Hz, which would speed up significantly the execution of the optimization algorithm.

Further work includes the exploitation of *a priori* knowledge in at least two directions. On one hand, qualitative information on the effect of the manipulated variables could be used to improve the tuning algorithm, similarly to [33,34]. On the other hand, a large collection of data, comprising FelQFactor time series along with the corresponding control variables, as manipulated by the machine experts, could be exploited to infer tuning rules by machine learning algorithms.

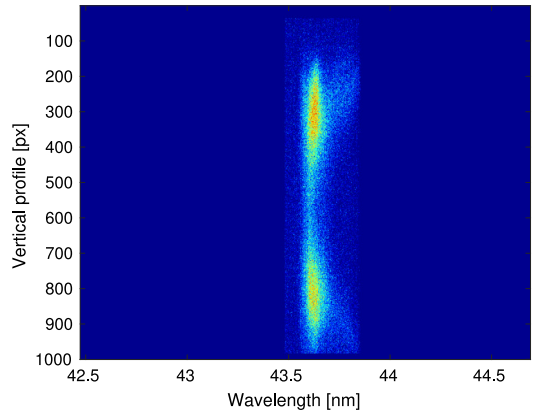

(a) Initial spectrum.

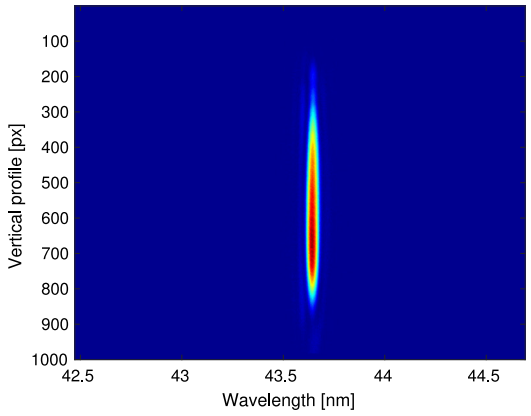

(b) Final spectrum.

Fig. 17. Spectrum before Fig 17(a) and after Fig 17(b) optimization with the stochastic extremum seeking method.

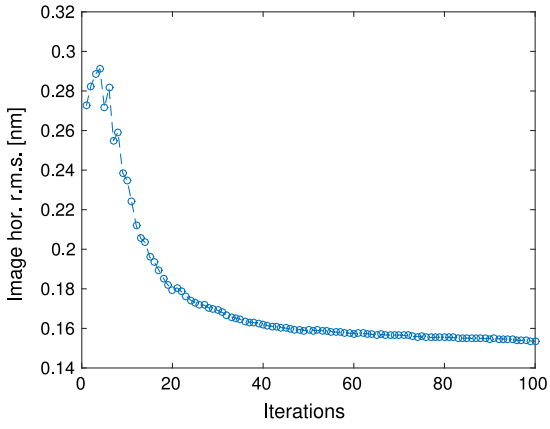

(a) Bandwidth.

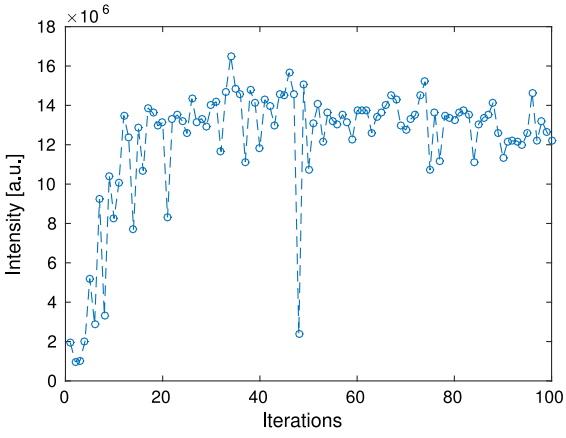

(b) Intensity.

Fig. 18. Stochastic extremum seeking method: variation of spectrum bandwidth and intensity during the iterations.

Acknowledgments

The authors wish to thank the FERMI machine physics team for the support and assistance during the tests, and in particular E. Allaria, L. Giannessi and G. Penco for their comments and suggestions to improve the quality of the paper.

Appendix A. Supplementary data

Supplementary material related to this article can be found online at http://dx.doi.org/10.1016/j.nima.2017.07.048.

References

[1] L.H. Yu, Generation of intense UV radiation by subharmonically seeded single-pass free-electron lasers, Phys. Rev. A 44 (8) (1991) 5178.

[2] E. Allaria, et al., The FERMI free-electron lasers, J. Synchrotron. Radiat. 22 (3) (2015) 485–491.

[3] E. Allaria, et al., Highly coherent and stable pulses from the FERMI seeded free-electron laser in the extreme ultraviolet, Nat. Photon. 6 (10) (2012) 699–704.

[4] E. Allaria, et al., Two-stage seeded soft-X-ray free-electron laser, Nat. Photon. 7 (11) (2013) 913–918.

[5] G. Gaio, M. Lonza, Evolution of the FERMI beam based feedbacks, in: Proc. ICALEPCS, 2013, pp. 1362–1365.

[6] M. Lonza, et al., Status report of the FERMI@Elettra control system, Proc. ICALEPCS 2011, Grenoble, France (2011).

[7] E. Allaria, et al., Two-colour pump–probe experiments with a twin-pulse-seed extreme ultraviolet free-electron laser, Nat. Commun. 4 (2013).

[8] K.C. Prince, et al., Coherent control with a short-wavelength free-electron laser, Nat. Photon. 10 (3) (2016) 176–179.

[9] I. Agapov, G. Geloni, I. Zagorodnov, Statistical optimization of FEL performance, Proc. IPAC2015, Richmond, VA, USA (2015).

[10] S. Tomin, I. Agapov, W. Colocho, T. Cope, A. Egger, Y. Fomin, G. Geloni, Y. Krylov, D. Ratner, A. Valentinov, et al., Progress in automatic software-based optimization of accelerator performance, in: 7th International Particle Accelerator Conference (IPAC'16), Busan, Korea, May 8-13, 2016, JACOW, Geneva, Switzerland, 2016, pp. 3064–3066.

[11] M. McIntire, T. Cope, S. Ermon, D. Ratner, Bayesian optimization of FEL performance at LCLS, in: Proceedings of the 7th International Particle Accelerator Conference, 2016.

[12] Ilya Agapov, G. Geloni, S. Tomin, I. Zagorodnov, Automatic tuning of free electron lasers, ArXiv Preprint ArXiv:1704.02335 (2017).

[13] G. Gaio, M. Lonza, Automatic FEL Optimization at FERMI, in: 15th Int. Conf. on Accelerator and Large Experimental Physics Control Systems (ICALEPCS'15), Melbourne, Australia, 17–23 October 2015, JACOW, Geneva, Switzerland, 2015, pp. 26–29.

[14] C. Svetina, D. Cocco, N. Mahne, L. Raimondi, E. Ferrari, M. Zangrando, PRESTO, the on-line photon energy spectrometer at FERMI: design, features and commissioning results, J. Synchrotron. Radiat. 23 (1) (2016) 35–42.

[15] L. Saule, Valutazione automatica della qualità dello spettro di un free electron laser mediante analisi di immagini, bachelor's thesis, Università degli Studi di Trieste (2015).

[16] J. Matas, O. Chum, M. Urban, T. Pajdla, Robust wide-baseline stereo from maximally stable extremal regions, Image Vis. Comput. 22 (10) (2004) 761–767.

[17] P. Diaconis, R.L. Graham, Spearman's footrule as a measure of disarray, J. R. Stat. Soc. Ser. B Stat. Methodol. (1977) 262–268.

[18] N. Bruchon, Algoritmi di controllo per la massimizzazione delle prestazioni di un laser a elettroni liberi, master's thesis, Università degli Studi di Trieste (2016).

[19] Y. Tan, W.H. Moase, C. Manzie, D. Nei, I.M.Y. Mareels, Extremum seeking from 1922 to 2010, in: Proceedings of the 29th Chinese Control Conference, 2010, pp. 14–26.

[20] M. Krsti, Encyclopedia of Systems and Control, Springer London, London, ISBN: 978-1-4471-5058-9, 2015, pp. 413–417. http://dx.doi.org/10.1007/978-1-4471-5058-9_114.

[21] J.-Y. Choi, M. Krsti, K.B. Ariyur, J.S. Lee, Extremum seeking control for discrete-time systems, IEEE Trans. Automat. Control (ISSN: 0018-9286) 47 (2) (2002) 318–323. http://dx.doi.org/10.1109/9.983370.

[22] S.Z. Khong, D. Nei, Y. Tan, C. Manzie, Unified frameworks for sampled-data extremum seeking control: global optimisation and multi-unit systems, Automatica (ISSN: 0005-1098) 49 (9) (2013) 2720–2733. http://dx.doi.org/10.1016/j.automatica.2013.06.020. http://www.sciencedirect.com/science/article/pii/S0005109813003348.

[23] C. Manzie, M. Krsti, Extremum seeking with stochastic perturbations, IEEE Trans. Automat. Control (ISSN: 0018-9286) 54 (3) (2009) 580–585. http://dx.doi.org/10.1109/TAC.2008.2008320.

[24] S.J. Liu, M. Krsti, Stochastic averaging in continuous time and its applications to extremum seeking, in: Proceedings of the 2010 American Control Conference, (ISSN: 0743-1619), 2010, pp. 172–177. http://dx.doi.org/10.1109/ACC.2010.5530487.

[25] D. Nei, A. Mohammadi, C. Manzie, A framework for extremum seeking control of systems with parameter uncertainties, IEEE Trans. Automat. Control (ISSN: 0018-9286) 58 (2) (2013) 435–448. http://dx.doi.org/10.1109/TAC.2012.2215270.

[26] A. Scheinker, Extremum Seeking for Stabilization, University of California, San Diego, 2012.

[27] A. Scheinker, M. Krsti, Minimum-seeking for CLFs: universal semiglobally stabilizing feedback under unknown control directions, IEEE Trans. Automat. Control (ISSN: 0018-9286) 58 (5) (2013) 1107–1122. http://dx.doi.org/10.1109/TAC.2012.2225514.

[28] A. Scheinker, X. Pang, L. Rybarcyk, Model-independent particle accelerator tuning, Phys. Rev. Accel. Beams 16 (10) (2013) 102803.

[29] A. Scheinker, M. Bland, M. Krsti, J. Audia, Extremum seeking-based optimization of high voltage converter modulator rise-time, IEEE Trans. Control Syst. Technol. (ISSN: 1063-6536) 22 (1) (2014) 34–43. http://dx.doi.org/10.1109/TCST.2013.2240387.

[30] A. Scheinker, S. Baily, D. Young, J.S. Kolski, M. Prokop, In-hardware demonstration of model-independent adaptive tuning of noisy systems with arbitrary phase drift, Nuclear Instruments and Methods in Physics Research Section a: Accelerators, Spectrometers, Detectors and Associated Equipment (ISSN: 0168-9002) 756 (2014) 30–38. http://dx.doi.org/10.1016/j.nima.2014.04.026. http://www.sciencedirect.com/science/article/pii/S0168900214004227.

[31] A. Scheinker, S. Gessner, Adaptive method for electron bunch profile prediction, Phys. Rev. Accel. Beams 18 (10) (2015) 102801.

[32] A. Scheinker, X. Huang, J. Wu, Minimization of betatron oscillations of electron beam injected into a time-varying lattice via extremum seeking, IEEE Trans. Control Syst. Technol. (ISSN: 1063-6536) PP (99) (2017) 1–8. http://dx.doi.org/10.1109/TCST.2017.2664728.

[33] F. Blanchini, G. Fenu, G. Giordano, F.A. Pellegrino, Plant tuning: A robust Lyapunov approach, in: Decision and Control (CDC), 2015 IEEE 54th Annual Conference on, IEEE, Osaka, 2015, pp. 1142–1147. http://dx.doi.org/10.1109/CDC.2015.7402365.

[34] F. Blanchini, G. Fenu, G. Giordano, F.A. Pellegrino, Model-free plant tuning, IEEE Trans. Automat. Control (ISSN: 0018-9286) 62 (6) (2017) 2623–2634. http://dx.doi.org/10.1109/TAC.2016.2616025.